AEROSOL OPTICAL DEPTH FROM SPECTRAL DIRECT NORMAL IRRADIANCE MEASUREMENTS IN MONTEVIDEO, URUGUAY

P. Russo[a *], A. Laguarda[b], G. Abal[a, b], L. Doppler[c]

[a]Laboratorio de Energía Solar (LES), Universidad de la República, Salto, Uruguay - (paolarussoganon, gonzalo.abal)@gmail.com
[b]Laboratorio de Energía Solar (LES), Universidad de la República, Montevideo, Uruguay - agu.laguarda@gmail.com
[c]Deutscher Wetterdienst, Berlin, Germany - lionel.doppler@dwd.de

KEY WORDS: Aerosol Optical Depth, Solar Spectral Irradiance, AERONET, Retrieval.

ABSTRACT:

Aerosols are liquid or solid particles with diameters between 2.5 and 10 µm suspended in the lower layers of the atmosphere. Aerosol Optical Depth (AOD) is a relevant parameter that quantifies their concentration in the atmosphere. It is usually estimated from sun photometer measurements at specific wavelengths. The objective of this work is to implement a simple inversion algorithm to retrieve AOD at six different wavelengths (340, 380, 440, 500, 675 and 870 nm) using solar direct normal spectral irradiance ground measurements from a relatively low cost collimated spectroradiometer (EKO MS-711) at a low-altitude site in Montevideo, Uruguay. The results obtained are compared with AERONET products for the same site, including AOD and Angström coefficient. The results of AOD for all wavelengths show a consistent negative mean bias (MBD, unitless), between -0.005 and -0.015, and dispersion (RMSD, unitless) between 0.021 and 0.015 (to be compared to a mean reference AOD of 0.097). These metrics improve considerably for very clear days, MBD up to $\pm$ 0.001 and RMSD under 0.007 (to be compared to a mean reference AOD of 0.058). These results are considered to be a first step in implementing the methodology and acquiring local knowledge about AOD retrievals using relatively simple instrumentation.

1. INTRODUCTION

Aerosols is a generic term that refers to solid or liquid suspended particles in the lower layers of the atmosphere, typically with diameters between 2.5 and 10 µm. They can be originated by natural sources as volcano eruptions, dust storms, sea salt, etc., or by anthropogenic sources as pollutant emissions and biomass burns. Their concentration, size distribution and optical properties play an important role in several areas, such as the Earth's energy balance (Chen et al., 2010), cloud formation (Seinfeld et al., 2016), human health (Johannson et al., 2015) and atmospheric radiative processes in general affecting the solar irradiance reaching the ground surface (Gueymard and Ruiz-Arias, 2016). Their measurement and monitoring using simple instrumentation is key in the efforts to advance in climate action and sustainable development objectives.

Aerosol Optical Depth (AOD) is a quantification of the radiative extinction (due to scattering and absorption) caused by aerosol content in a vertical column of the atmosphere, at a specific wavelength (WMO/GAW, 2016). The most common technique used to estimate AOD consists of measuring the monocrhomatic solar direct normal irradiance, and estimating the attenuation that occurs between the top of the atmosphere (TOA) and the surface level, using a combination of the law of exponential attenuation (Lambert-Beer-Bouguer Law) and the Langley Plot method (Holben et al., 1998; Giles et al., 2019) to estimate the intensity of the direct normal irradiance that the same instrument would have measured at TOA. This approach uses an inversion algorithm which implies a well-characterized understanding of the other attenuation processes involved, such as Rayleigh scattering and attenuation by gas absorption. While traditionally sun photometers have been used for this purpose, the advancements in commercial spectroradiometers have made them a viable alternative to retrieve AOD with acceptable accuracy. For instance, in recent research (García-Cabrera et al., 2020; Qiao et al., 2023; Gröbner and Kouremeti, 2019), an EKO MS-711 collimated spectroradiometer was used to retrieve AOD at multiple wavelengths, demonstrating that it is possible to obtain accurate AOD estimates with a commercial spectroradiometer. The procedure used is similar than the one used in this work (described in Section 2), and the results are shown in Table 1.

	MBD		RMSD	
λ (nm)	García	Quiao	García	Quiao
340	0.007	na	<0.001	na
380	0.005	0.003	<0.001	0.026
440	0.005	-0.011	0.001	0.024
500	0.005	<0.001	0.002	0.020
675	0.006	0.009	<0.001	0.021
870	0.003	-0.012	<0.001	0.020

Table 1. Comparison of retrieved AOD_λ from EKO MS-711 measurements against AERONET estimates (García-Cabrera et al., 2020; Qiao et al., 2023). Performance is evaluated with the mean bias deviation (MBD, unitless) and the root mean squared deviation (RMSD, unitless), relative to the reference mean values.

The objective of this work is to retrieve AOD at six different wavelengths: 340, 380, 440, 500, 675 and 870 nm, using solar direct normal spectral irradiance ground measurements from a collimated spectroradiometer (EKO MS-711) at the AERONET site in Montevideo, Uruguay, and evaluate the accuracy of the AOD estimates, using as reference the AOD reported by AERONET at the same site. The method selected to be implemented is an inversion algorithm that combines the Lambert Beer Bouguer Law with the Langley Plot Method, and the wavelengths of interest are selected in order to match the AOD products of AERONET database.This work is a first a approach on the subject and aims to acquire local knowledge about the retrieval of AOD with this equipment in particular, to then be

able to estimate AOD from solar spectral irradiance measurements in other sites of the region were there is no availability of a sun photometer (for instance, there is only one AERONET site in Uruguay).

2. METHODOLOGY

The methodology used to estimate AOD is schematized in Figure 1. Spectral irradiance measurements of the solar beam are taken with an EKO MS-711 DNI spectroradiometer of wavelength range: 300-1100 nm, at 1-minute frequency.

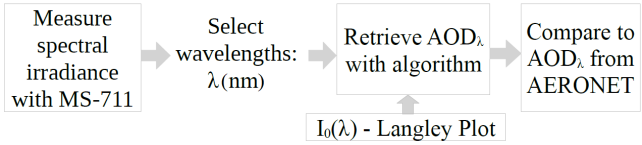

Figure 1. Methodology scheme.

The measurements are taken at the rooftop of the College of Engineering in Montevideo, Uruguay (latitude = -34.9182°, longitude = -56.1665°, altitude = 58 m.a.s.l.), were the AERONET measurements with the sun photometer are routinely made. The period considered is during spring in the southern hemisphere, from September to November, 2022. The spectroradiometer MS-711 has a wavelength interval of 0.3–0.5 nm, a Full Width at Half Maximum (FWHM) < 7 nm and a Field of View or FOV = 5°. The measured spectral irradiance is interpolated to 1 nm intervals, using linear interpolation. Figure 2 shows the spectral irradiance measured (blue) at one example instant and the vertical lines (green) indicate the wavelengths of interest for the AOD retrieval. The instrument is mounted on an EKO STR-22G sun tracker that uses a GPS sensor and sun sensor system for accurately tracking the sun. Since the FOV captures an area larger than the solar disc, some circumsolar irradiance is counted as beam irradiance, because of this a circumsolar correction is included in the inversion algorithm.

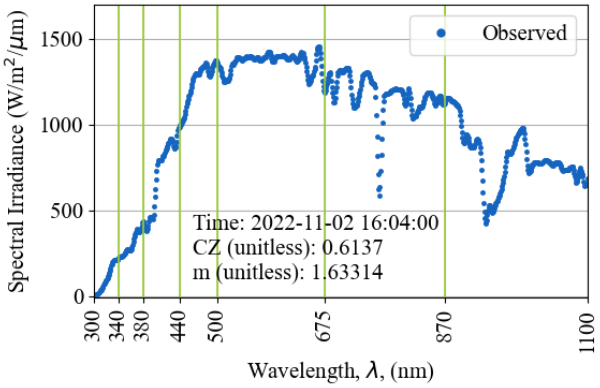

Figure 2. Example of measured spectral irradiance.

2.1 Data Used

To apply the inversion algorithm, each irradiance measurement selected must simultaneously comply:

i) correspond to clear-sky and stable atmospheric conditions

ii) have a simultaneous AERONET measurement available

iii) passing strict visual inspection to discard instants that could correspond to unstable atmospheric conditions, cirrus clouds, erroneous measurements.

AERONET measurements of 1.5 quality level already include a clear sky selection (Holben et al., 1998), in this work that selection is double checked with an automated clear sky selection algorithm based on Reno and Hansen (2016) criteria, using the auxiliary Global Horizontal Irradiance (GHI) measurements, plus visual inspection on the integral of the direct normal spectral irradiance measured. Furthermore, once the preliminary Aerosol Optical Depth, $\tau_{a,i}(\lambda)$, is retrieved for every wavelength, a manual post processing stage is applied, to discard instants where $\tau_{a,i}(\lambda)$ shows anomalous values and this coincides with suspiciously unstable sky conditions in the integral of the direct normal spectral irradiance.

The final selection consists of 2629 instants from 46 different days. These are distributed in the morning (26%), noon (29%) and afternoon (45%) (Figure 3).

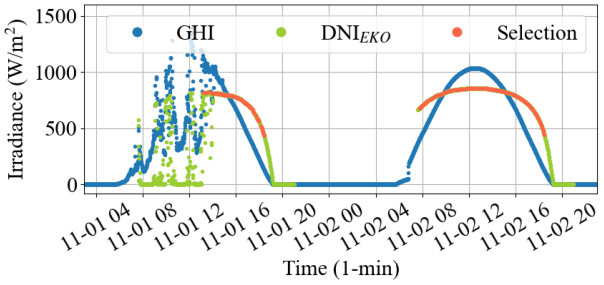

Figure 3. Selection of clear-sky instants for two sample days (November 1 and 2, 2022).

AERONET

The Aerosol Robotic Network (AERONET, `https://aeronet.gsfc.nasa.gov/`) from NASA (Holben et al., 1998) has a measurement station in Uruguay, located at Montevideo (in the same rooftop where this study is being performed). The site is equipped with a CIMEL sun photometer with FWHM of 10 nm for all wavelengths, except for 340 and 380 nm where it is 2 and 4 nm respectively. Its FOV is 1.2°. Regarding aerosols, the variables used from AERONET are AOD at wavelengths 340, 380, 440, 500, 675, 870 nm, as well as the Angström exponent, α, between each two wavelengths. This network also provides information of the site pressure in hPa and the total column content of ozone (O_3) and Nitrogen Dioxide (NO_2) (but these last two come originally from the Ozone Monitoring Instrument, OMI).

2.2 Inversion Algorithm

The law of exponential attenuation (Lambert-Beer-Bouguer) states

$$I(\lambda) = I_0(\lambda)\, e^{-m\tau(\lambda)} \tag{1}$$

where: $I(\lambda)$ is the solar beam spectral irradiance measured at ground level. $I_0(\lambda)$ is the spectral irradiance at the top of the atmosphere. It is computed as $I_0(\lambda) = I_s(\lambda) \times F_n$ where I_s is the reference solar spectral irradiance estimated using the Langley Plot method (Subsection 2.4) and F_n is the orbital correction factor. In Eq. (1), m is the relative air mass and $\tau(\lambda)$ the total optical depth.

Contributions to attenuation are: Rayleigh scattering (r), aerosols (a), water vapor (H_2O), absorption by atmospheric gases NO_2, O_3 and O_2:

$$\tau(\lambda)\, m = \tau_r(\lambda)\, m_r + \tau_a(\lambda)\, m_a + \tau_{H_2O}(\lambda)\, m_{H_2O} + \tau_{NO_2}(\lambda)\, m_{NO_2} + \tau_{O_3}(\lambda)\, m_{O_3} + \tau_{O_2}(\lambda)\, m_{O_2} \quad (2)$$

The relevant absorptions for the required wavelenghts are described in Table 2. Note that, for these particular wavelenghts, water vapor plays a negligible role (Giles et al., 2019).

Wavelength, nm	Optical depths
340	τ_r, τ_{NO_2}, τ_{O_3}
380	τ_r, τ_{NO_2}
440	τ_r, τ_{NO_2}
500	τ_r, τ_{NO_2}, τ_{O_3}
675	τ_r, τ_{O_3}
870	τ_r

Table 2. Relevant optical depths considered in Eq. (1), for each wavelength of study.

The relative air masses corresponding to each relevant process are calculated as follows. The inverse air mass related to Rayleigh scattering is (Kasten and Young, 1989)

$$m_r^{-1} = \cos\theta + 0.50575 \times (96.07995 - \theta_{deg})^{1.6364} \quad (3)$$

where θ is the solar zenith angle (radians) and θ_{deg} is its expression in degrees. The inverse air mass related to the NO_2 optical depth (Gueymard, 1995) is

$$m_{NO_2}^{-1} = \cos\theta + 602.30 \times \theta_{deg}^{0.5}\,(117.960 - \theta_{deg})^{-3.4536} \quad (4)$$

The inverse air mass related to aerosols (Kasten, 1964) is

$$m_a^{-1} = \cos\theta + 0.1500 \times (93.885 - \theta_{deg})^{-1.253} \quad (5)$$

and the air mass related to Ozone (Komhyr and Grass, 1989) is

$$m_{O_3} = \left[1 - \left(\frac{R + h_s}{R + h}\right)^2 \sin^2\theta\right]^{-1/2} \quad (6)$$

where $R = 6371.229$ km is the mean radius of the Earth, $h = 22$ km is the mean height of the stratospheric ozone layer and h_s is the station height above mean sea level, in this case $h_s = 0.058$ km.

Regarding the optical depths, Rayleigh optical depth is calculated as (Hansen and Travis, 1974)

$$\tau_r(\lambda) = \frac{p}{p_0} \cdot \frac{0.008569}{\lambda^4} \times \left(1 + \frac{0.0113}{\lambda^2} + \frac{0.00013}{\lambda^4}\right) \quad (7)$$

where $p_0 = 101.325$ kPa is the atmospheric pressure at sea level, p is the measured atmospheric pressure in kPa at the site and λ the wavelength in µm. The Nitrogen Dioxide optical depth is the product of its column density and its absorption cross section,

$$\tau_{NO_2}(\lambda) = u_{NO_2} \cdot \sigma_{NO_2}(\lambda) \quad (8)$$

where u_{NO_2} (molecules/cm^2) is the nitrogen dioxide column obtained from AERONET and $\sigma_{NO_2}(\lambda)$ (cm^2/molecules) is the absorption cross section for NO_2 obtained from HITRAN (Rothman et al., 1992), as the average of the cross sections corresponding to 220 K and 294 K. Similarly, the optical depth for Ozone is

$$\tau_{O_3}(\lambda) = u_{O_3} \cdot \sigma_{O_3}(\lambda) \quad (9)$$

Where the total Ozone column (u_{O_3} in cm^2/molecules) is given by AERONET. The absorption cross section for O_3, $\sigma_{O_3}(\lambda)$ in cm^2/molecules, for $\lambda = 340$ nm is obtained from HITRAN, using the average of the cross sections corresponding to 5 temperatures (193, 213, 253, 273, 293 Kelvin) and for λ = 500 and 675 nm, it is as given in (Burrows et al., 1999).

Finally, the aerosol optical depths at each of the relevant wavelengths, AOD_λ or $\tau_a(\lambda)$, are obtained from the corresponding $I(\lambda)$ measurement and Eqs. (1) and (2).

2.3 Circumsolar Correction

The EKO spectroradiometer has a FOV (Field of View) of 5° and, as mentioned before, the CIMEL sun photometer used by Aeronet has a FOV of 1.2°. The FOV recommended by WMO for AOD retrievals is less or equal to 2.5° (WMO/GAW, 2004). Thus, a larger portion of circumsolar radiation is counted as DNI by the EKO instrument. A circumsolar correction is applied to attenuate this effect. It consists in subtracting from the measured DNI spectral irradiance, $I_{obs}(\lambda)$ (W/m^{2}µm), an estimation of the circumsolar portion (CSR, W/m^{2}µm), to obtain an estimate of the spectral irradiance that comes from within 1.2° of the Sun-Earth direction, $I(\lambda)$, as shown in Eq. (10). The circumsolar ratio is the % of observed spectral irradiance that is circumsolar, i.e. $CR = CSR/I_{obs}(\lambda)$. This ratio depends on the FOV of the instrument and the $\text{AOD}_{\lambda,i}$ during the particular instant i, as shown in Figure 4, in this case CR is from García-Cabrera et al. (2020) and the $\text{AOD}_{\lambda,i}$ is from AERONET.

$$I(\lambda) = I_{obs}(\lambda) - CSR \quad (10)$$

The procedure for correcting the measured spectral irradiance is simple. At each instant i, using the $\text{AOD}_{\lambda,i}$ from AERONET and Figure 4, a CR_i (%) value is obtained and the circumsolar contribution, CSR_i, is estimated. Finally, the measured irradiance is corrected to obtain the estimated irradiance from Eq. (10) or, equivalentely, from $I(\lambda) = I_{obs}(\lambda)(1 - CR)$. For high aerosol loads and low wavelengths CR may be 0.05, as shown in Figure 4.

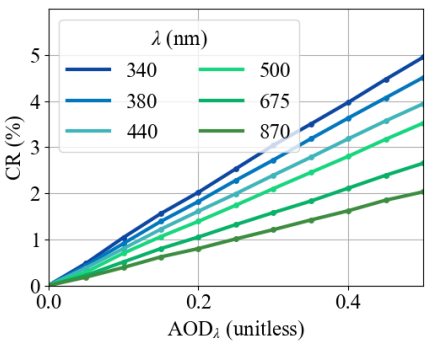

Figure 4. Estimated circumsolar ratio, CR (expressed as %), depending on the AOD_λ level, extracted from García-Cabrera et al. (2020).

2.4 TOA Spectral Irradiance

The reference solar spectral irradiance that the instrument would have measured at the top of the atmosphere, $I_s(\lambda)$ is estimated applying the Langley Plot method. This method uses Eq. (1) to obtain

$$\ln\left[\frac{I_i(\lambda)}{F_{n,i}}\right] = \ln\left[I_s(\lambda)\right] - \tau_i(\lambda)\, m_i \qquad (11)$$

where the index i denotes the timestamp (or "instant") of the measurement. Assuming a nearly constant total optical depth, τ_i, the Eq. (11) implies a linear dependence between the logarithm of the spectral irradiance with the air mass. The linear coefficient is $a = -\tau_i(\lambda)$, and the independent term $b = \ln[I_s(\lambda)]$. The Langley Plot method requires stable atmospheric conditions for its validity, so it must be applied over short periods of time and under clear-sky conditions. In a period, a least squares regression provides optimal values for a and b. Finally, $I_s(\lambda) = e^b$. This procedure is commonly called the calibration of the instrument. It is recommendable (Cuevas et al., 2019) to have very low AOD during the instants selected to calibrate the instrument, for example, CIMEL sun photometers from Aerosol Robotic Network (AERONET) at Mauna Loa Observatory or PFR sun photometers from Global Atmospheric Watch (GAW) at Izaña Observatory, are typically calibrated under conditions of $0.01 < \mathrm{AOD}_{500} < 0.02$. In this study, the range of AOD_λ (AERONET) during the instants used for the calibration is shown in Table 3.

In this work, the Langley Plot method is applied to the measurements made during the clearest day selected, 2^{nd} of November 2022, within 1-hour intervals, to obtain I_{s_j} estimates for the j^{th} interval of steady atmospheric conditions. This day is selected because it has the lowest AOD conditions and the highest correlation coefficients (R^2) in each period, thus the points have good alignment and small errors in the linear regression, assuring it is valid to apply the Langley Plot Method. The Langley plots for two wavelengths in one example period, from 16:00 to 17:00 hs, are shown in Figure 5. The value of I_s used in the inversion algorithm is the average value between the I_{s_j} obtained that had the highest coefficient of determination (R^2). The final estimates for $I_s(\lambda)$ and their standard deviation are shown in Table 3.

λ, nm	$I_s(\lambda)$, W/m^{2}µm	periods	σ (%)	AOD_λ range
340	773.4	5*	4.1	0.059-0.062
380	979.7	8	2.6	0.061-0.066
440	1605.3	8	3.1	0.054-0.059
500	1869.6	8	2.3	0.049-0.059
675	1377.3	5	2.1	0.038-0.042
870	1217.9	4	1.1	0.030-0.034

Table 3. Spectral irradiance at TOA ($I_s(\lambda)$) used in this work. The values are obtained as the average of the Langley Plot method over short periods intervals during 2022/11/02. The number of short periods, the standard deviation, σ (expressed as percentage of I_s) and the range of the reference AOD_λ (AERONET) are reported in the last three columns. *I_s at 340 nm was also composed with two periods from other clear days.

For the I_s (λ) values to be considered acceptable, an additional criteria is used, that consists of checking that the difference between AOD_λ retrieved in this work and AOD_λ from AERONET complies with Eq. (12) for more than 95% (U_{95}) of the instants used to find I_s, as recommended in WMO/GAW (2004). Figure 6 shows the AOD_λ calculated in this work, using the $I_s(\lambda)$ obtained, minus the AOD_λ taken as reference (AERONET), during the instants used for the calibration. Different colours and markers correspond to the six different wavelengths and the grey curves correspond to the lower and upper limits of the U_{95} criteria. As a result, more than 95% of the points fall within the

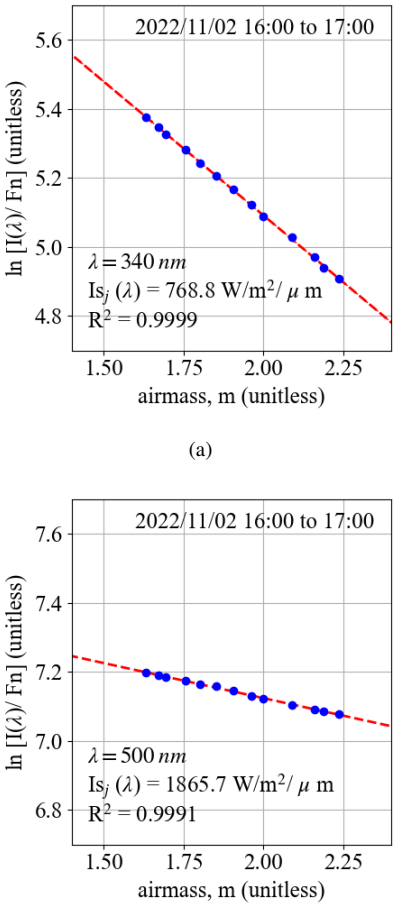

Figure 5. Langley plots at wavelengths = 340 and 500 nm, for one sample period.

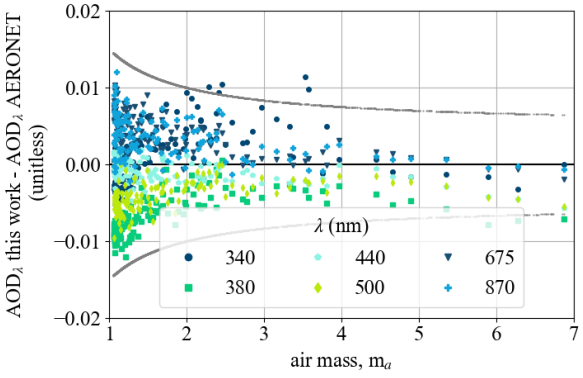

Figure 6. U_{95} criteria (WMO/GAW (2004), Eq. (12)) applied at every wavelength, to determine if the values of I_s (λ) estimated return $\mathrm{AOD}_{\lambda,i}$ that fall within the acceptability limits: $\pm(0.005 + 0.010/m_a)$, during the instants used for calibration.

acceptance limits, during the instants used for the calibration.

$$U_{95} < 0.005 + 0.010/m_a \tag{12}$$

2.5 Performance Metrics

The metrics used to analyze the accuracy of the AOD estimations are the Mean Bias Deviation (MBD, unitless) and the Root Mean Squared Deviation (RMSD, unitless). The MBD is defined as

$$\text{MBD} = \frac{1}{N}\sum_{i=1}^{i=N}\left[\tau_{a,i}(\lambda) - \text{AOD}_{\lambda,i}\right], \tag{13}$$

where N is the number of estimates, $\tau_{a,i}$ is the aerosol optical depth obtained in this study for a given time i and $\text{AOD}_{\lambda,i}$ are the corresponding reference estimates from AERONET. A positive value of MBD indicates a systematic overestimation (or underestimation if negative). The RMSD, defined as

$$\text{RMSD} = \left[\frac{1}{N}\sum_{i=1}^{i=N}\left[\tau_{a,i}(\lambda) - \text{AOD}_{\lambda,i}\right]^2\right]^{1/2} \tag{14}$$

indicates the average dispersion of the errors. The mean reference AOD_λ from AERONET and the mean AOD_λ from this work are also reported.

3. RESULTS

Aerosol optical depth for wavelengths 340, 380, 440, 500, 675 and 870 nm was retrieved from 2629 spectroradiometer measurements using the methodology described in Section 2. The performance metrics for these results are shown in Table 4, including in the last column the mean value from AERONET used as a reference. The dispersion as quantified by the RMSD is similar to those reported for other sites shown in Table 1. However, a significant underestimation is apparent at all wavelengths.

λ (µm)	MBD (unitless)	RMSD (unitless)	AOD_λ This work	AOD_λ AERONET
340	-0.005	0.015	0.121	0.126
380	-0.015	0.021	0.107	0.122
440	-0.010	0.017	0.097	0.107
500	-0.013	0.019	0.082	0.095
675	-0.006	0.016	0.066	0.072
870	-0.006	0.015	0.054	0.060

Table 4. Performance results with circumsolar correction, for the whole period (2629 instants)

There is a large variability in the results between different days. Table 5 shows the performance results for the clearest day selected (November 2^{nd} 2022). For this day, the RMSD are significantly lower (below 0.007, unitless), and the bias also decreases in absolute terms but with alternating signs indicating under-estimations and over-estimations at different wavelengths.

Figure 7 shows the MBD (unitless) for every wavelength with error bars of ± RMSD (unitless) for the whole period (blue) and for the clearest day (turquoise). For each case, the average MBD is indicated as a dashed horizontal line. Biases for the clearest day are lower at every wavelength and their average is very close to zero. The dispersion (RMSD) is also lower. The wavelengths of the best performance during the clearest day are close to the UV (340 and 440 nm) with bias under ± 0.001 (unitless) and dispersion under 0.004 (unitless), followed by 500, 870, 380 and 675 nm, which are still considered good since biases are within ± 0.006 (unitless) for all cases.

λ (µm)	MBD (unitless)	RMSD (unitless)	AOD_λ This work	AOD_λ AERONET
340	0.001	0.004	0.070	0.069
380	-0.006	0.007	0.066	0.072
440	-0.001	0.002	0.063	0.064
500	-0.004	0.004	0.054	0.058
675	0.004	0.005	0.050	0.046
870	0.003	0.004	0.042	0.038

Table 5. Performance results with circumsolar correction, for the clearest day selected: November 2^{nd} 2022, based on 125 instants.

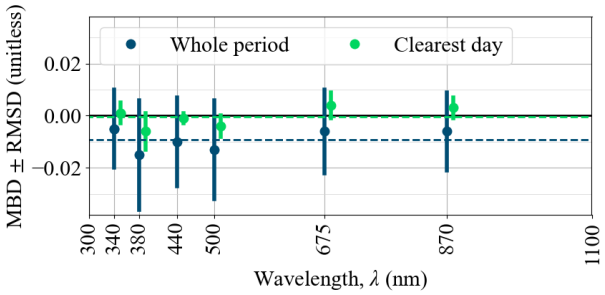

Figure 7. Results of MBD and RMSD for the whole period and for the clearest day. The error bars are ± RMSD (unitless).

Figure 8 shows the scatter diagrams for AOD at each wavelength. The absolute frequency is coded in color (yellow represents higher frequency), so each plot can be read as a 2D histogram. From a qualitative point of view there is a good agreement between AOD retrieved from the MS-711 and the reference AOD from AERONET. The negative bias (underestimation) is apparent in each scatter plot.

Ångström Parameters

The Ångström equation

$$\tau_a(\lambda) = \beta\,\lambda^{-\alpha} \tag{15}$$

where λ is in µm, describes approximately the dependence of the AOD with λ, where α is known as the Ångström exponent and β the optical depth at $\lambda = 1$ µm, (sometimes referred to as atmospheric turbidity parameter). The Ångström exponent, α, is related to aerosol size with values greater than 2 indicating small particles associated with combustion byproducts, and values less than 1 indicating large particles like sea salt and dust (Schuster et al., 2006).

The Ångström parameters can be estimated, under stable atmospheric conditions, using $\tau_a(\lambda)$ at two or more wavelengths, since Eq. (15) implies a linear dependence between $\ln[\tau_a(\lambda)]$ and $\ln\lambda$, with independent term $\ln(\beta)$ and slope $-\alpha$.

This methodology is applied to the pair of aerosol optical depths: $\tau_a(\lambda = 440\,\text{nm})$ and $\tau_a(\lambda = 870\,\text{nm})$ and their corresponding wavelengths, at every instant. The slope and intercept are found by linear regression, obtaining α_i, then α is calculated as the average for the period.

The average values obtained for the day 2022/11/02 are reported in the second line of Table 6 and compared to the average

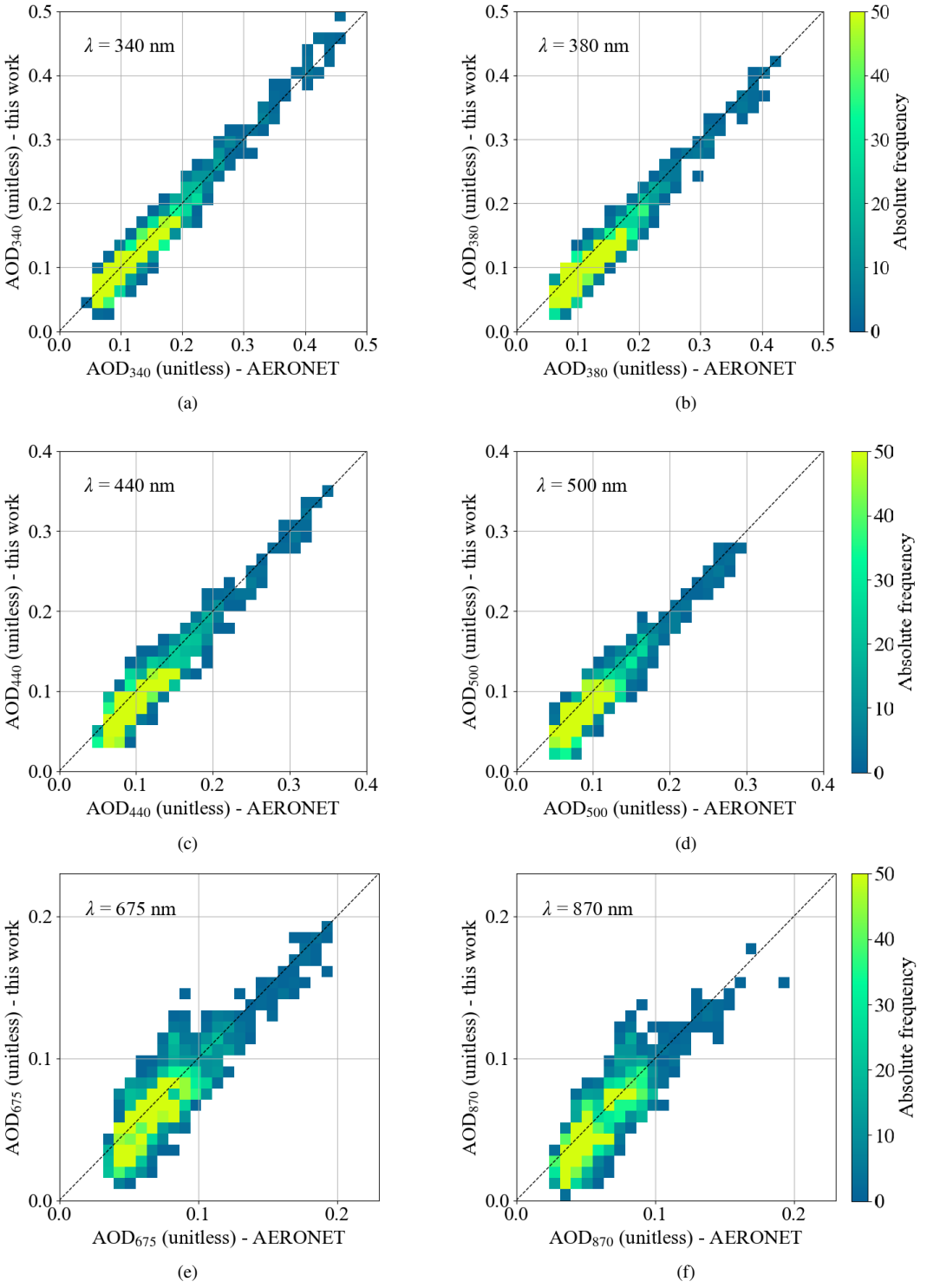

Figure 8. AOD_λ retrieved vs. AOD_λ AERONET, 2D histograms.

of the instantaneous values reported by AERONET for the same day. The same procedure is applied to the range 340-440 nm and the results are also reported in Table 6. The estimated value for 340-440 nm is higher than the AERONET value, and for 440-870 nm it is lower, the difference is considered to be small and related to the biases presented in AOD_λ. Furthermore, it should be noted that the instantaneous values of α_i include a variability in each instant and for each wavelength, that is then transferred as uncertainty in the final averaged α. Regarding the values obtained, Montevideo is a coastal urban site, so it is expected to have a small Ångström exponent associated to larger particles (for example dust and sea salt).

Since there are AOD_λ at several wavelengths, it is also possible to verify that the Ångström's Law is valid, especially when there are aerosols of dust type. This is done by checking the linearity of the the logarithm of AOD_λ against the logarithm of λ. Figure 9 shows the results of this procedure applied to the average AOD_λ's of the day 2022/11/02, obtaining $R^2 = 0.99$.

interval index	wavelength range (nm)	α this work	α AERONET
1	340-440	0.403	0.319
2	440-870	0.623	0.762

Table 6. Ångström exponents α from this work vs. AERONET (average for the clearest day).

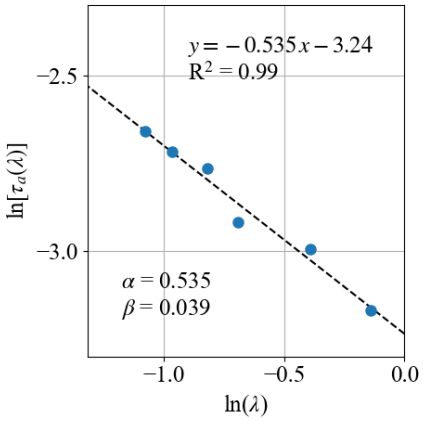

Figure 9. Ångström's Law validity, for the average AOD_λ's from the clearest day selected (2022/11/02).

4. CONCLUSIONS AND DISCUSSION

Aerosol optical depth (AOD) at 6 wavelengths (340, 380, 440, 500, 675 and 870 nm) was successfully retrieved from solar direct normal spectral irradiance measurements at one site in Uruguay for a 46-day period. The measurements were made with an EKO MS-711 spectroradiometer, a commercially available and relatively low-cost instrument. The inversion algorithm used is based on the law of exponential attenuation and uses the Langley Plot method over a selected day (2022/Nov/02) to obtain the spectral irradiance that the instrument would measure at the top of the atmosphere. A circumsolar correction procedure was applied to compensate for the relatively large field of view (FOV) of the EKO instrument with respect to AERONET sun photometers.

The AODs obtained were compared to AERONET estimations based on a CIMEL Sun photometer for the same site. A performance with dispersions (RMSD, unitless) between 0.015 and 0.021 was obtained, and a consistent negative bias (MBD, unitless) between -0.005 and -0.015 was observed at all wavelengths and during the whole period (to be compared to a mean AOD of 0.097), indicating an underestimation of AOD's from EKO measurements. For the clearest day selected (2022/Nov/02), the performance improves considerably, with MBD's of $\pm$ 0.001 for 340 and 440 nm, and in the $\pm$ 0.006 range for the worst cases (at 380, 500 and 675 nm). The dispersion (RMSD) remains below 0.007 for this day (to be compared to a mean AOD of 0.058). These results are comparable to those from previous works (Table 1), which also include circumsolar corrections.

The performance of the AOD results is strongly affected by the extraterrestrial spectral irradiance estimate for the instrument, $I_s(\lambda)$. This parameter is estimated using the Langley Plot method. It is preferable to estimate $I_s(\lambda)$ using measurements performed at high altitude sites, under very stable atmospheric conditions and with very low AOD. In our case, the measurement site is located essentially at sea level (height is 56 m asl) and the altitude of Uruguay is below 600 m over all its territory, so it was not possible to perform high altitude measurements. In order to estimate $I_s(\lambda)$ with acceptable precision, a strict selection of the instants used in the calibration was made, selecting low AOD conditions and double checking the clear sky and stability conditions. Applying this methodology, it was possible estimate values of $I_s(\lambda)$ for the six wavelengths, and use them to retrieve AOD_λ that met the acceptability limits U_{95} recommended (WMO/GAW, 2004; Kazadzis et al., 2017) (this implies that during the instants used for the calibration, the differences between AOD_λ from this work and AOD_λ from AERONET were within $\pm 0.005 + 0.010/m_a$, for more than 95% of the samples). For this reason, the results are considered satisfactory for a preliminary calibration, however, it is noted that in international comparisons, for full compliance of the traceability recommendations, more than 1000 measurements with AOD_{500} between 0.04 and 0.2 should be considered, and a minimum of five days of measurements.

The performance metrics (bias and dispersion) improved significantly for a selected clear sky day with very stable atmospheric conditions. This suggests that instants with trace cirrus clouds or variable conditions might be selected and the small fluctuations in the irradiance can reflect as errors in the AOD estimates. Since the AOD inversion algorithm is only valid for clear sky instants, it is important to precisely detect the clear sky instants and discard false positives.

Regarding the simple circumsolar correction procedure applied, it improved significantly the AOD_λ estimates, particularly in the higher AOD_λ values for each wavelength. It is recommendable to incorporate it in retrievals based on instruments with FOV's larger that 2.5°.

These preliminary results for AOD retrieved from low-cost measurements look promising. Future improvements to this methodology include correcting the negative bias, improving the clear sky and stable atmospheric conditions selection, expanding the number of sites to other AERONET locations and comparing with other satellite data sources. In particular, the negative bias of the AODs estimates over all wavelengths during the period can be associated to the $I_s(\lambda)$ estimated, which shows large uncertainties. This can be improved by a larger set of measurements, in which more short periods with clear sky, stable atmospheric conditions and low AOD_λ become available. This problem will be addressed in future work exploring different alternatives for the calibration methodology (Campanelli et al., 2007).

ACKNOWLEDGEMENTS

The author P. Russo would like to thank the National Oceanic and Atmospheric Administration (NOAA, U.S. Department of Commerce), for the invaluable opportunity to participate in ISRSE-39 in Antalya, Turkey, particularly to Dir. Dr. S. Volz, Dep. Dir. M. A. Kutny and Mr. M. Zandbergen. To the organization of the conference, particularly to Dr. D. Klein and Ms. A. Yeşilırmak. To Deutscher Wetterdienst (DWD), particularly to Dr. L. Doppler and Dr. S. Wacker for kindly providing their time, support and knowledge to advance with the calculus methodology. To the National Agency of Investigation and Innovation (ANII) for the awarded MSc. scholarship to study this subject as a part of the Thesis. To Dr. E. Frins for the kindly shared workspace at Montevideo AERONET station, and to the

colleagues from the Solar Energy Laboratory (LES), particularly Dir. Dr. R. Alonso for the continuous encouragement and help, and MSc. I. Piccioli for his collaboration with the measurement campaign.

REFERENCES

Burrows, J. P., Richter, A., Dehn, A., Deters, B., Himmelmann, S., Voigt, S., Orphal, J., 1999. Atmospheric remote-sensing reference data from GNOME-2. Temperature-dependent Absorption Cross Sections of O_3 in the 231-794nm Range. *Journal of Quantitative Spectroscopy and Radiative Transfer*, 61(4), 509–517.

Campanelli, M., Estellés, V., Tomasi, C., Nakajima, T., Malvestuto, V., Martínez-Lozano, J. A., 2007. Application of the SKYRAD Improved Langley plot method for the in situ calibration of CIMEL Sun-sky photometers. *Applied Optics*, 46(14), 2688–2702.

Chen, W. T., Nenes, A., Liao, H., Adams, P., Li, J., Seinfeld, J., 2010. Global climate response to anthropogenic aerosol indirect effects: Present day and year 2100. *Journal of Geophysical Research: Atmospheres*, 115(D12).

Cuevas, E., Romero-Campos, P. M., Kouremeti, N., Kazadzis, S., Räisänen, P., García, R. D., Barreto, A., Guirado-Fuentes, C., Ramos, R., Toledano, C., Almansa, F., Gröbner, J., 2019. Aerosol optical depth comparison between GAW-PFR and AERONET-Cimel radiometers from long-term (2005–2015) 1 min synchronous measurements. *Atmospheric Measurement Techniques*, 12(8), 4309–4337.

García-Cabrera, R. D., Agullo, E., Barreto, A., Cachorro, V. E., Pó, M., Ramos, R., Hoogendijk, K., 2020. Aerosol retrievals from the EKO MS-711 spectral direct irradiance measurements and corrections of the circumsolar radiation. *Atmospheric Measurement Techniques*, 13(5), 2601–2621. https://amt.copernicus.org/articles/13/2601/2020/.

Giles, D., Sinyuk, A., Sorokin, M., Schafer, J., Smirnov, A., Slutsker, I., Eck, T., Holben, B., Lewis, J., Campbell, J., Welton, E., Korkin, S., Lyapustin, A., 2019. Advancements in the Aerosol Robotic Network (AERONET) Version 3 database – automated near-real-time quality control algorithm with improved cloud screening for Sun photometer aerosol optical depth (AOD) measurements. *Atmospheric Measurement Techniques*, 12, 169–209.

Gröbner, J., Kouremeti, N., 2019. The Precision Solar Spectroradiometer (PSR) for direct solar irradiance measurements. *Solar Energy*, 185, 199-210.

Gueymard, C., 1995. Smarts2, simple model of the atmospheric radiative transfer of sunshine: Algorithms and performance assessment. Technical Report Rep. FSEC-PF-270-95,, Florida Solar Energy Center.

Gueymard, C. A., Ruiz-Arias, J. A., 2016. Extensive worldwide validation and climate sensitivity analysis of direct irradiance predictions from 1-min global irradiance. *Solar Energy*, 128, 1–30. Special issue: Progress in Solar Energy.

Hansen, J. E., Travis, L. D., 1974. Light scattering in planetary atmospheres. *Space Sci. Rev.*, 16, 527–610.

Holben, B., Eck, T., Slutsker, I., Tanré, D., Buis, J., Setzer, A., Vermote, E., Reagan, J., Kaufman, Y., Nakajima, T., Lavenu, F., Jankowiak, I., Smirnov, A., Gueymard, C., 1998. AERONET-A Federated Instrument Network and Data Archive for Aerosol Characterization. *Remote Sensing of Enviroment*, 66, 1–16.

Johannson, K. A., Balmes, J. R., Collard, H. R., 2015. Air pollution exposure: a novel environmental risk factor for interstitial lung disease? *Chest*, 147(4), 1161-1167.

Kasten, F., 1964. Technical report 136 - a new table and approximation formula for the relative optical air mass. Physical publication, U.S. Army Material Command, Cold Regions Research and Engineering Laboratory, Hanover, New Hampshire.

Kasten, F., Young, A., 1989. Revised optical air mass tables and approximation formula. *Applied Optics*, 28(22), 4735–4738.

Kazadzis, S., Kouremeti, N., Gröbner, J., 2017. Fourth wmo filter radiometer comparison (frc-iv). Technical report, Physikalisch-Meteorologisches Observatorium Davos, World Radiation Center.

Komhyr, W. D., Grass, R. D., 1989. Dobson Spectrophotometer 83': A Standard for Total Ozone Measurements, 1962-1987. *Journal of Geophysical Research*, 94, 9847–9861.

Qiao, C., Liu, S., Huo, J., Mu, X., Wang, P., Jia, S., Fan, X., Duan, M., 2023. Retrievals of precipitable water vapor and aerosol optical depth from direct sun measurements with EKO MS711 and MS712 spectroradiometers. *Atmospheric Measurement Techniques*, 16(6), 1539–1549. https://amt.copernicus.org/articles/16/1539/2023/.

Reno, M., Hansen, C., 2016. Identification of periods of clear sky irradiance in time series of GHI measurements. *Renewable Energy*, 90, 520–531.

Rothman, L., Gamache, R., Tipping, R., Rinsland, C., Smith, M., Benner, D., Devi, V., Flaud, J., Camy-Peyret, C., Perrin, A., Goldman, A., Massie, S., Brown, L., Totht, R., 1992. The HITRAN molecular database: Editions of 1991 and 1992. *Journal of Quantitative Spectroscopy and Radiative Transfer*, 48, 469–507.

Schuster, G., Dubovik, O., Holben, B., 2006. Angstrom exponent and bimodal aerosol size distributions. *Journal of Geophysical Research*, 111, D07207.

Seinfeld, J. H., Bretherton, C., Carslaw, K. S., Coe, H., DeMott, P. J., Dunlea, E. J., Feingold, G., Ghan, S., Guenther, A. B., Kahn, R., Kraucunas, I., Kreidenweis, S. M., Molina, M. J., Nenes, A., Penner, J. E., Prather, K. A., Ramanathan, V., Ramaswamy, V., Rasch, P. J., Ravishankara, A. R., Rosenfeld, D., Stephens, G., Wood, R., 2016. Improving our fundamental understanding of the role of aerosol-cloud interactions in the climate system. *Proceedings of the National Academy of Sciences*, 113(21), 5781-5790.

WMO/GAW, 2004. Experts workshop on a global surface-based network for long term observations of column aerosol optical properties. Technical Report 162, WMO/GAW.

WMO/GAW, 2016. Aerosol measurement procedures, guidelines and recommendations. Technical report, WMO/GAW.